REVISION 2

IN SITU RAMAN SPECTROSCOPIC STUDY OF TRANSIENT POLYHEDRAL DISTORTIONS DURING CESIUM ION EXCHANGE INTO SITINAKITE

Aaron J. Celestian*, Michael Powers, and Shelby Rader

Advanced Materials Institute, Department of Geography and Geology, Western Kentucky University, Bowling Green, Kentucky 42101, USA

* corresponding author: aaron.celestian@wku.edu

ABSTRACT

The Na-form of the synthetic counterpart of the mineral sitinakite (sitinakite-Na) has been studied in situ for the ion exchange systems of Na→Cs and Na→H→Cs using time-resolved Raman spectroscopy. Raman spectral mode analysis was performed based on a comparative study of previous titanium silicate Raman spectroscopy, as well as time-resolve X-ray diffraction studies. The Raman spectrum of sitinakite can be broken down to three main groups of bending and stretching modes: Ti-O-Ti, Si-O-Ti, and O-Ti-O bends between 200 cm^{-1} and 400 cm^{-1}; and Ti-O stretch between 400 cm^{-1} and 625 cm^{-1}. During Na-form to H-form ion exchange, rapid red shifts were observed in absolute peak positions, as well as relative changes between peak positions, indicating a symmetry change. TiO_6 polyhedral groups distort as hydroxyl groups form on the TiO_6 octahedra. Upon Cs exchange into the H-form, a rapid, two-step blue shift was observed for all peak positions, which indicated that the 8 membered-ring becomes more circular. Upon Cs exchange into the Na-form, slow changes of peaks in the Raman spectrum indicated up to four discrete polyhedral distortions during ion exchange. The advantage of Raman spectroscopy in this study was the observation of transient polyhedral distortions for the initial swelling of sitinakite while immersed in deionized H_2O and during H and Cs ion exchange in the crystal structure. Previous X-ray diffraction studies were not of sufficient resolution to model H_2O swelling effects and framework polyhedral distortions during ion exchange, thus Raman spectroscopy offers a complimentary tool to measure changes in framework geometry in situ during ion

exchange. The results presented here are directly relevant to other ion exchange research on titanium silicates, zirconium silicates, aluminum silicates, and aluminum phosphates. Additionally this work shows the usefulness of *in operando* experiments, conducted in deliberately variable environments, which can monitor the molecular dynamics of a system, collect information concerning structure-response mechanisms, and capture the catalytic parameters for the reaction/process.

INTRODUCTION

Ion exchange in zeolites and other microporous materials has broad ranging applications, including water purification, gas separation, catalysis, and heavy cation sequestration. One particularly beneficial application is the selective sequestration of Cs and Sr from aqueous solutions. Spent nuclear fuel produces large quantities of high- and low-level radioactive waste, where the majority the radioactivity is generated by ^{90}Sr and ^{137}Cs (Wilmarth et al., 2011). In addition, Cs and Sr are generated in low concentrations (10^{-3} to 10^{-5} M) (Zheng et al., 1995), and the wastes can be highly alkaline (Anthony et al., 1994; Pertierra et al., 1999; Wilmarth et al., 2011). Sr and Cs removal results in a reduction of the overall radioactivity of the solutions. It is most advantageous that candidate host materials for Sr and Cs be highly ion selective, resist molecular degradation from high gamma radiation doses, and be thermally stable to at least 400°C (Galloway et al., 2006; Thorogood et al., 2010).

The mineral sitinakite ($HNa_2KTi_4Si_2O_{14}•4H_2O$), a microporous material, successfully removes Cs and Sr ions from an aqueous media (Celestian et al., 2010, and references therein). Sitinakite (also known as CST or TS in the literature, for crystalline silicotitanate or titanium silicate, respectively) is found predominantly in mines of northern Russia (Khibiny Massif, Kola Peninsula), where it crystallizes in hydrothermal systems (Menshikov et al., 1992). Despite the scarcity of the mineral in nature, sitinakite can easily be synthesized in large quantities in the laboratory from a basic Na gel. Sitinakite-Na (the synthesized Na-form of the material) crystallizes in tetragonal space group, $P4_2/mcm$, with unit-cell parameters of a≈7.8 Å and c≈11.9 Å (Poojary et al., 1994). The framework structure can be described as edge-shared TiO_6 octahedra forming a columnar structure trending along the *c*-axis. These TiO_6 columns are linked by SiO_4 tetrahedral groups in the *ab*-plane (Fig. 1). The resulting structure generates 8-

membered-rings (8MR) consisting of four SiO_4 and four TiO_6 groups running parallel to [001], and perpendicular 6-membered-rings (6MR) along [010]. The negatively charged framework must be neutralized by cations residing within the 8MR and/or 6MR channels. Cations of large ionic radius (> 1.0 Å, e.g. K, Rb, Cs) can only reside in the larger 8MR (diameter of ≈6.5 Å) and are typically bound to molecular H_2O. Cations of small ionic radius (≤1.0 Å, e.g. Li, Na, rare earth elements) are able to reside in the 6MR or 8MR channels.

Previous diffraction studies of Cs exchange into sitinakite have demonstrated that the exchange mechanisms involve multiple steps serve to enhance and promote ion selectivity in this material (Celestian and Clearfield, 2007; Celestian et al., 2008; Celestian et al., 2005; Celestian et al., 2010). There are two crystallographically distinct Na sites. Site Na1 is situated in the 6MR channel and site Na2 is situated in the 8MR channel on the (110) mirror and approx. 0.7 Å from the 4_2-axis along [001]. Previous studies had indicated that H exchange into sitinakite-Na occurred faster that data collection could resolve, and therefore it was unknown how the Na was removed. However, H pre-exchange allows for fast Cs ion exchange (< 2.5 min.), whereas the exchange process is >2 hrs. (at a flow rate ≈ 2 mL/min. and ≈10 mM CsCl) if Cs is exchanged directly into sitinakite-Na. Once the sitinakite is H exchanged, the structure of sitinakite transforms from space group $P4_2/mcm$ to $P4_2/mbc$ and the 8MR channels become elliptical. Cs ion exchange occurred quickly into sitinakite-NaH, but did so in two distinct steps involving H levers in the structure. The first lever was the hydration of the ingoing Cs cation into the crystallographic site designated as Cs2 (Fig. 1). This hydration forced the positive dipole of the H_2O to rotate and move closer to the proton on the framework O^{2-}. The second lever was the repulsion of the OH group on the framework that forced the channel to become circular. Once the channel was circular, a second ion exchange site (Cs1 – Fig. 1) became the favored ion exchange site. When Cs was exchanged directly into the Na-form, the exchange process occurred in two steps, however the mechanisms were different due to the presence of competing ions in the 8MR channel rather than OH groups attached to the framework, and a different H-bond network scheme (Celestian et al., 2010). The first exchange step of Cs exchange into sitinakite-Na was the replacement site Na1 in the 8MR with the simultaneous dehydration of H_2O site OW2. After dehydration, and subsequent disruption of the hydrogen bonding network, site Cs1 quickly filled. Those works demonstrated that ion exchange diffusion is a multi-step process and strongly depends on the initial host cation type, as well and the H-bond network of H_2O/OH groups.

X-ray diffraction is effective for modeling long-range atomic arrangements, chemical site occupancies, and absolute structural configurations. Time-resolved X-ray or neutron diffraction studies of ion exchange processes in molecular sieves usually require the use the high flux sources such as synchrotrons or isotope reactors/spallation neutron sources, respectively. Static exchange experiments are typically used to evaluate if ion exchange is possible for a chemical system, but the rates and dynamics of the ion exchanges cannot be measured. With in situ Raman spectroscopy however, snapshots of molecular conformational changes in the framework can be measured in near real-time during the exchange process without the immediate requirement of high flux X-rays or neutrons. A disadvantage of Raman spectroscopy is that the assignments of Raman active modes are not known *a priori* for many mineral systems, and must be inferred by Raman comparison studies as has been done for microporous titanium silicate and related materials (Ferdov et al., 2008; Hess et al., 2001; Kostov-Kytin et al., 2005; Liu et al., 2010; Nash et al., 2007; Pavel et al., 2007; Ricchiardi et al., 2001; Southon and Howe, 2002; Su et al., 2000; Zhang et al., 2010). In some cases, density functional theory can be used to calculate Raman shift and the intensity of molecular vibrational modes and successfully correlated to mineral structures with small unit cell volume and high symmetry (e.g. Arroyabe et al., 2011; Kaindl et al., 2011; Kaindl et al., 2012; Tobbens and Kahlenberg, 2011). If mode assignments can be made, in situ Raman microscopy can be used for rapid monitoring of molecular dynamics and kinetics prior to using synchrotron or neutron sources that are used for atomic structure refinement.

This study presents a comparative analysis of ion exchange in sitinakite using in situ Raman spectroscopy and previously published time-resolved X-ray diffraction to resolve ambiguities associated with the disruption of H-bond networks and transient polyhedral distortions in the sitinakite structure. Goals of this study include determining if transient molecular changes occur during the ion exchange process where time-resolved XRD could not model, and correlating time-resolved Raman spectra with previous XRD (Celestian et al., 2008; Celestian et al., 2010) to generate qualitative band assignments for future ion exchange studies in microporous titanium silicates.

METHODS

Synthesis of Sitinakite-Na

The sodium-form of sitinakite (sitinakite-Na) was synthesized as follows. Approximately 23.75 mL of deionized H_2O was added to a 250 mL Nalgene bottle. While stirring with a magnetic stir plate, 6.6 mL of Ti-isopropoxide

was added drop-wise, after which a thick precipitate formed and was left to stir for approximately one minute. Then 40 mL of H_2O_2 was added, covered loosely, until the mixture turns dark red (approximately 2 minutes). 150 mL of deionized H_2O was added quickly and let stir for several minutes. The pH was then adjusted to approximately 11 by drop-wise addition of 10 M NaOH. Once the pH reached approximately 11, AS-40 (colloidal silica) was added drop-wise to the gel until the pH was between 12.5 and 13.0. Teflon-lined Parr autoclaves were filled halfway with the gel and heated at 215 °C for one week. The crystals were filtered and rinsed with deionized H_2O and set aside to air dry at ambient temperature. Powder X-ray diffraction using a Rigaku Miniflex II (Cu Kα), a JEOL 120CX transmission electron microscopy using, and a JEOL 5400LV scanning electron microscope showed sitinakite as the only phase present with crystals measuring between approximately 20 nm to 2 μm on edge (Fig. 2A, 2B). The advantage of this synthesis over other published versions of sitinakite and the Nb-doped variant (e.g. Anthony et al., 1995; Anthony et al., 2002; Cherry et al., 2004; Chitra et al., 2011; Luca et al., 2002; Medvedev et al., 2004; Milne et al., 2006; Pertierra et al., 1999; Poojary et al., 1996; Poojary et al., 1994; Tripathi et al., 2005) is only one vessel is used for the duration of the procedure, no overly dangerous procedures are performed (although personal protective equipment should be worn at all times and chemical safety training is required prior to experimentation), and no impurities were found in the product.

Ion Exchange Setup

Ion exchange solutions were prepared at room temperature and ambient pressure. The HCl solution was made by adding 5 mL of stock HCl to 95 mL of deionized H_2O to make an approximate 0.6 M HCl solution. A 100 mL 0.01 M CsCl solution was prepared (0.168 g of CsCl in 100 mL deionized H_2O) in preparation for in situ Raman studies.

A vacuum environmental cell (Fig. 2C) was developed to allow for combined time-resolved and stop-flow experiments. Suitably sized crystals could be taken out of the cell for single crystal diffraction studies and then placed back in the cell for continued time-resolved spectroscopic work. The cell was constructed in-house and designed to minimize the beam path through the ion exchange solution and maximize the single to noise ratio during data collection. The flow rate of the exchanging solution was held constant for the entire duration of the experiment using a Masterflex peristaltic pump set to 2 mL/min. At 2 mL/min, 5 min elapsed before the exchange solution came in contact with the sample.

Raman Spectroscopy

A Thermo DXR dispersive Raman microscope with a 780nm diode laser at a power of 14 mW, a Peltier-cooled CCD detector and a high-resolution diffraction grating (< 3 cm^{-1} resolution between 50 cm^{-1} to 1800 cm^{-1}) was used for all experiments in this study. Laser frequency and laser spot position were calibrated using a polystyrene standard, and the spectrometer was calibrated using excitation lines from a neon lamp. Exposures for the Na→H→Cs exchange were 10 sec with 3 acquisitions each (total time 30 sec/spectrum). Exposures for the Na→Cs exchange were 60 sec with 3 acquisitions each (total time 3 min/spectrum). Exposure times varied because of the different uptake rates known for this exchange system. The microscope and laser settings were held constant for all experiments, set at 50 μm laser slit (orthoscopic), 50x (0.5 N.A.) long-working distance objective and laser spot size at the sample estimated to be 1.1 μm. A total of 400 spectra were collected for each experiment (varying between a total experimental time of 200 min. and 1200 min, depending on spectrum acquisition rate), smoothed using a Savitzky-Golay algorithm (Savitzky and Golay, 1964) (5 points, 2.411 cm^{-1}), and both the original data and the processed data were saved as separate ascii files.

Both exchange experiments began with dry sitinakite samples, which were then wetted with deionized H_2O. For the Na→H→Cs experiment, HCl followed the H_2O to replace Na with H. The HCl solution did not reach the sample until minute 5 (spectrum 10), and was allowed to pass through the sample for an additional 5 minutes (spectrum 20). This step ensured complete H-exchange, as determined by previous X-ray diffraction studies (Celestian et al., 2008; Celestian et al., 2007). Finally, the exchange solution was changed by moving the advection line from the HCl solution to the CsCl solution. The CsCl solution did not reach the sample until 5 minutes later (minute 15, spectrum 30), and was allowed to flow continuously until the end of the experiment. The Na→Cs exchange experiment proceeded directly from H_2O to CsCl solution. The CsCl solution did not reach the sample unit minute 5 (end of spectrum 2) and was allowed to continuously flow until the end of the experimental run.

Our peak evaluation strategy was to first perform iterative-targeted transformation factor analysis on the entire time series data for each experiment to estimate the number of individual components contributing to the spectrum, followed by individual peak fitting for selected regions in the time series data. The ITTFA was advantageous for quantitative evaluation of peak intensity and position as a function of time. In this manor, even small variations in trends of peak intensity or position could be assigned to individual components. Once each component was

separated into its own spectrum using the ITTFA, we assigned the vibrational modes (discussed later) based on those changing peak intensities and positions. Several curve fitting software products were applied to fit the Raman spectra in the ranges 280-320 cm^{-1} and 480-620 cm^{-1}, using Lorentzian, pseudoVoigt, or Gaussian shaped peak functions with variable and fixed full width half-maximum (FWHM) parameters. In most cases the obtained peak positions (discussed later) were negligibly affected by the fitting procedure. Thus for simplicity and reproducibility we have used Gaussian peak shapes, which is consistent with the submicron mean size of the crystallites (Smit et al., 2003), and FWHMs fixed to the corresponding refined FWHM parameters for sitinakite prior to the ion exchange. The data presented in this paper were obtained using the PeakFit scripts for Matlab. The total numbers of peak positions chosen were the minimum number that yielded a good fit (RMS of ~2 or less).

RESULTS AND DISCUSSION

All possible Raman active modes for sitinakite could not be distinguished in the collected Raman spectra, therefore the absolute mode assignment of vibrational bands was not possible. Raman active modes were grouped into three categories based on a time-resolved powder XRD studies of Cs into the fully exchanged H-form (sitinakite-NaH) (Celestian et al., 2008), Cs exchange into sitinakite-Na (Celestian et al., 2010), empirical Raman mode assignments made by Su, Balmer, and Bunker (2000) (Su et al., 2000), and other previous work (Ferdov et al., 2008; Hess et al., 2001; Kostov-Kytin et al., 2005; Liu et al., 2010; Mihailova et al., 1996; Nash et al., 2007; Pavel et al., 2007; Ricchiardi et al., 2001; Southon and Howe, 2002). Group α was defined in this study as the suite of peaks in the region from 200 cm^{-1} to 400 cm^{-1}. Profile fitting using a constant width Gaussian function showed there were two peaks for Group α and six peaks for Group β (Figs. 3 and 4). Group α likely represents the bending vibrational modes of Si-O-Ti and Ti-O-Ti polyhedra, which is a measure of the channel elipticity and the connectivity of the titania groups. Group β was defined in this study as the region from 400 cm^{-1} to 625 cm^{-1} and likely represents the TiO_6 stretching modes, which is a measure of the distortion in the titania polyhedra. Group χ from 700cm^{-1} to 1050 cm^{-1}, not discussed further, are likely the Si-O stretching modes. Peak changes and migrations in this study, and compared to other studies (Su et al., 2000), give confidence to the assignment of spectral groups to structural groups in sitinakite.

182

183 ***In situ ion exchange: the Na to H to Cs forms***

184 Time-resolved Raman spectra for the sitinakite Na→H→Cs exchange experiment showed significant changes
185 during ion diffusion (Figs. 5, 6, 7, 8). Relative changes between observed peak positions were used to indicate
186 molecular changes, specifically Ti-O-Si bending in the 8MR and O-Ti-O stretching in the TiO_6 octahedra, occurring
187 within the 8MR channel in sitinakite when compared to crystallographic properties determined from time-resolved
188 X-ray diffraction data. In the Group α region, difference peak analysis of the two most intense peaks (α1 and α2)
189 showed that sitinakite-Na underwent changes during flow of deionized H_2O prior to the HCl solution reaching the
190 sample (Fig. 7). The positional differences of peaks α1 and α2 (|α1-α2| Fig. 7) decrease from 31.5 cm^{-1} to 25.5 cm^{-1}
191 as deionized H_2O solution flowed over the sample. The immediate decrease in the |α1-α2| peaks upon immersion in
192 deionized H_2O was unexpected since there should be no ions in solution to induce an exchange effect and therefore
193 the framework polyhedral units should not change geometry. This initial decrease of the |α1-α2| could be caused by
194 an initial hydration of the sitinakite-Na, as H_2O uptake in the changes could force the Ti-O-Si and Ti-O-Ti to bend.
195 A separate experiment was performed to test the response of sitinakite-Na to immersion of deionized H_2O (data not
196 shown). Upon immersion in deionized H_2O, the |α1-α2| moved approximately 7 cm^{-1} closer together after 100 min.
197 of immersion. Upon removal and drying of the sitinakite-Na sample, the peaks returned to their starting values for
198 the dry sitinakite-Na. No changes to unit cell parameters were observed for sitinakite-Na immersion in deionized
199 H_2O in previous in situ time-resolved diffraction studies (Celestian et al., 2010).

200 When the HCl solution reached the sample at time 5 minutes (spectrum 10), the |α1-α2| positions moved closer, to a
201 difference of 13.5 cm^{-1}, and maintained these positions until the CsCl solution was introduced to the sample. Rapid
202 ion exchange was observed, and the rate of |α1-α2| decrease compares favorably with time-resolved XRD, where H
203 exchange occurred faster than data collection could monitor. As expected there was a large shift of the Ti-O-Si and
204 Ti-O-Ti bond angles between sitinakite-Na and sitinakite-NaH (Table 1), as seen in the shift in |α1-α2| to lower
205 wavenumbers.

206 At time 10 minutes (spectrum 20), the solution was changed from HCl to CsCl. Approximately 5 minutes (10
207 spectrum) after the exchange solution was changed to CsCl, the |α1-α2| increases from 13.5 cm^{-1} to 21cm^{-1} at

minute 15 (spectrum 30). The process took approximately 1.5 minutes (3 spectra), and the |α1-α2| peak positions held steady for approximately another 1.5 minutes (3 spectra). After 18.5 minutes (spectrum 37), the |α1-α2| began to slowly increase over 6.5 minutes (13 spectra) to an observed maximum of 24 cm^{-1}, where the positions remained for the rest of the experiment. All observed changes in the Group α region occurred within 25 minutes (50 spectra) from the start of the experiment. The experiment and data collection were allowed to continue for 3.75 hours, but no additional changes were observed. The above observations parallel the Cs occupancy kinetics based on time-resolved XRD diffraction study, as site Cs2 is filled rapidly, which occurs simultaneously with a structural transition that forces the 8MR geometry to become circular, and then followed by a slower diffusion of site Cs1 (Celestian et al., 2008). As with time-resolved XRD data, this Raman study showed a two-step conformational change during Cs uptake.

Group β likely represents the stretching modes of the TiO_6 polyhedra based on the results of previous comparative studies (Su 2000) and this study. The difference peak positions between the two most intense and well-resolved peaks in Group β, β3 and β5 (Fig. 8), show similar time dependent changes as the most intense peaks in Group ααι and α□. Within the first 5 minutes (first 10 spectra) the difference peak positions |β3-β5| decreased in the presence of deionized H_2O from 51.7 cm^{-1} to 42.0 cm^{-1}. After 5.5 minutes (spectrum 11), HCl reached the sample, the Δβ3β5 quickly increased to approx. 62.5 cm^{-1}, and held steady until the CsCl solution reached the sample 15 minutes (at spectrum 30) into the experiment. The change in the |β3-β5| peaks between the Na- and H-forms was expected, as the polyhedral distortion indices are significantly different (Table 1).

Upon Cs exchange, the |β3-β5| decreased to 51.0 cm^{-1} at minute 18 (spectrum 36) and then increased to approximately 53.5 cm^{-1} at minute 19.5 (spectrum 39), where it remained until the end of the experiment. The changes in |β3-β5| also occur in two steps, first a decrease and then an increase in relative |β3-β5| peak separation. At the end of the experiment, the |β3-β5| values are similar to the starting |β3-β5| values of the sitinakite-Na, indicating that the TiO_6 polyhedral geometry of the Na and Cs exchange forms are similar (within 2 wavenumbers). However, the calculated distortion indices of the TiO_6 polyhedron in sitinakite-NaHCs from the time-resolved X-ray structure refinements are significantly different than the indices in sitinakite-Na. Therefore the Raman spectrum of the Cs-form may indicate that the average crystallographic Ti site (or O^{2-} sites) of the framework in sitinakite is more symmetrically similar to those found in sitinakite-Na. Time-resolved X-ray scattering studies may not have

been of sufficiently high resolution to model the distorted polyhedral geometry in the Fourier difference maps (Celestian et al., 2008). The average bond length of sitinakite-Na and sitinakite-NaCs are different (Table 1), and this is also supported here by the absolute shift of all Group β peaks to lower wavenumbers (Fig. 6). Shifting peaks to lower wavenumbers is an indicator of increasing bond length (e.g. (Andrew et al., 1994; Huang et al., 2000)), which occurs as Cs diffuses into the structure. In addition, Raman spectroscopy revealed transient polyhedral distortions, which could not determined from X-ray data alone.

In situ ion exchange: the Na to Cs form

The Cs diffusion into sitinakite-Na was much slower than into sitinakite-NaH, as previously observed (Celestian et al., 2010). Because data capture rate was slower for this experiment, changes in spectra for H_2O uptake could not be as well resolved as in the Na→H→Cs experiment. Regardless, the magnitude of $|\alpha1-\alpha2|$ in the Na→Cs experiment is much smaller (< 2 cm^{-1}), compared to the changes observed in the Na→H→Cs experiment (~ 6 cm^{-1}). The time-resolved data and difference peak analysis (Figs. 9, 10, 11, 12) indicate a two-step ion diffusion process. The introduction of the CsCl solution caused the $|\alpha1-\alpha2|$ peak positions to change from a starting difference of 27 cm^{-1} to approximately 22.6 cm^{-1} over a time span of 45 minutes (at spectrum 15). Starting at minute 60 (spectrum 20), the $\Delta\alpha1\alpha2$ peak positions continuously increased and finally returned to the starting $|\alpha1-\alpha2|$ values of 27 cm^{-1} after 750 minutes (spectrum 250), where they remained to the end of the experiment (900 minutes, spectrum 300).

Previous time-resolved XRD of direct Cs exchange in sitinakite-Na indicated that no symmetry change or changes in 8MR geometry (Ti-O-Si and Ti-O-Ti bending) occur (Celestian et al., 2010). However, Raman data indicates that changes in the 8MR geometry occur immediately upon immersion in dilute CsCl solution (Fig. 11), as evidenced by a maximum shift of the low wavenumber peaks ($|\alpha1-\alpha2|$, peaks representing the Ti-O-Si and Ti-O-Ti bending modes) to 4.5 cm^{-1}. The structural significance of these changes is not currently quantified, but work is underway to solve these vibrational mode analyses using DFT (density functional theory) calculations. One possible cause of the $\alpha1$ and $\alpha2$ peak positions shift may be a change in the relatively short Cs2-O bond to the framework oxygen (approx. 3.06 Å). Raman data in this study indicate that upon initial ion exchange of Cs, the Cs2-O bond on the outside of the 8MR became shorter than previously modeled from XRD data. The shortening of the Cs2-O bond

would result in an elongation of the Ti-O bonds that bridge the Si sites, and a shortening of the Ti-O bonds that are bonded to other TiO_6 octahedra (cf. Pauling's second rule). This possible shorter Cs2-O bond and the lengthening of the Ti-O bonds to Si would distort the 8MR geometry without changing the space symmetry and result in a |α1-α2| peak migration. At the end of the Cs exchange into sitinakite-Na experiment, the starting |α1-α2| and ending |α1-α2| values are identical indicating that the 8MR geometry is similar, but the α1 and α2 peaks shift to lower wavenumbers (Figs. 9 and 11). This suggests that the 8MR has increased in size due to increased Ti-O-Si bonds as the large Cs cation exchanges into and expands the framework in the crystallographic *a* and *b* unit-cell parameters. The expansion of the *a* and *b* unit-cell parameters was also observed in the time-resolved XRD diffraction experiments.

The Group β□□□□□□□□s changed in a different pattern compared to Group α□□□□□□.12. The differences between the two strongest peaks (β5 and β3) had two distinct steps from minute 0 to 330, with a relatively rapid decrease of peak position difference from approximately 50.5 cm^{-1} to 47.5 cm^{-1} in the first 45 minutes (first 15 spectra), followed by a slow decrease to 45.9 cm^{-1} from minute 45 to minute 330 (spectrum 110). The next shift occurs between minutes 330 and 417 (spectra 110 and 139), where Δβ3β5 rapidly decreased from 45.9 cm^{-1} to 36.3 cm^{-1}. Finally, after minute 417 the Δβ3β5 began to increase back to near initial values of 50.5cm^{-1} by 900 minutes (spectrum 300) and held constant until minute 1200. The Group β showed an overall shift of peak positions to lower wavenumbers, but the |β3-β5| positions closely paralleled the Cs occupancy parameter from time-resolved XRD (Celestian et al., 2010), where Cs2 first filled the 8MR channel while H_2O slowly moved out of the 8MR. In this Raman Cs exchange study, there was an abrupt decrease (after 120 min.) and then an abrupt increase (after 140 min.) in the |β3-β5| peaks. These changes in the Raman spectra are coincident with the uptake of Cs into the Cs1 site that occurs after complete removal of H_2O from the Ow2 site in X-ray diffraction studies (Celestian et al., 2010). Cs1 and Ow2 sites occupy the same crystallographic position at the center of the 8MR and therefore cannot exist simultaneously. The slow induction time of Cs into site Cs2, which is disordered with the Na1 site, could result in distortions of the TiO_6 stretching modes because removed H_2O would strain the H-bond network. This dehydration effect by ion exchanging larger cations into the crystal structure could give rise to similar polyhedral distortions seen in zeolite dehydration (e.g. Wang and Bish, 2012). The TiO_6 polyhedral distortion is recovered upon Cs exchange into Cs1 as the Cs1 site bonds to the hydrogen donor framework O^{2-} sites and supports the

structure. The final |β3-β5| for the direct Cs exchange into sitinakite-Na is identical to the starting |β3-β5| (Fig. 13), indicating that the polyhedral geometries are similar. However, the decrease of the |β3-β5| peaks to lower wavenumbers suggests that the overall TiO_6 polyhedral volume had increased, which could account for the increase in the *a* and *b* unit-cell parameters (Celestian et al., 2010).

This study demonstrates that the extent of ion exchange can be determined precisely without prior knowledge of intermediate crystallography or crystal chemistry, and structural deformations, particularly the bending and stretching modes of low and high wavenumber regions for the H→Cs exchange here, can be measured with fast time resolution (in this case, 30 sec intervals). Future work in simultaneous Raman and XRD data collection coupled with density functional theory calculations of predicted molecular vibrational modes would offer an unprecedented view of ion exchange and other fast molecular-level mineral properties.

Acknowledgements: This work was funded in part by the WKU Advanced Materials Institute, J. Andersland for SEM and TEM images, NSF KY-EPSCoR, and for partial support in developing the environmental cell by the ACS-PRF # 50927-UNI10.

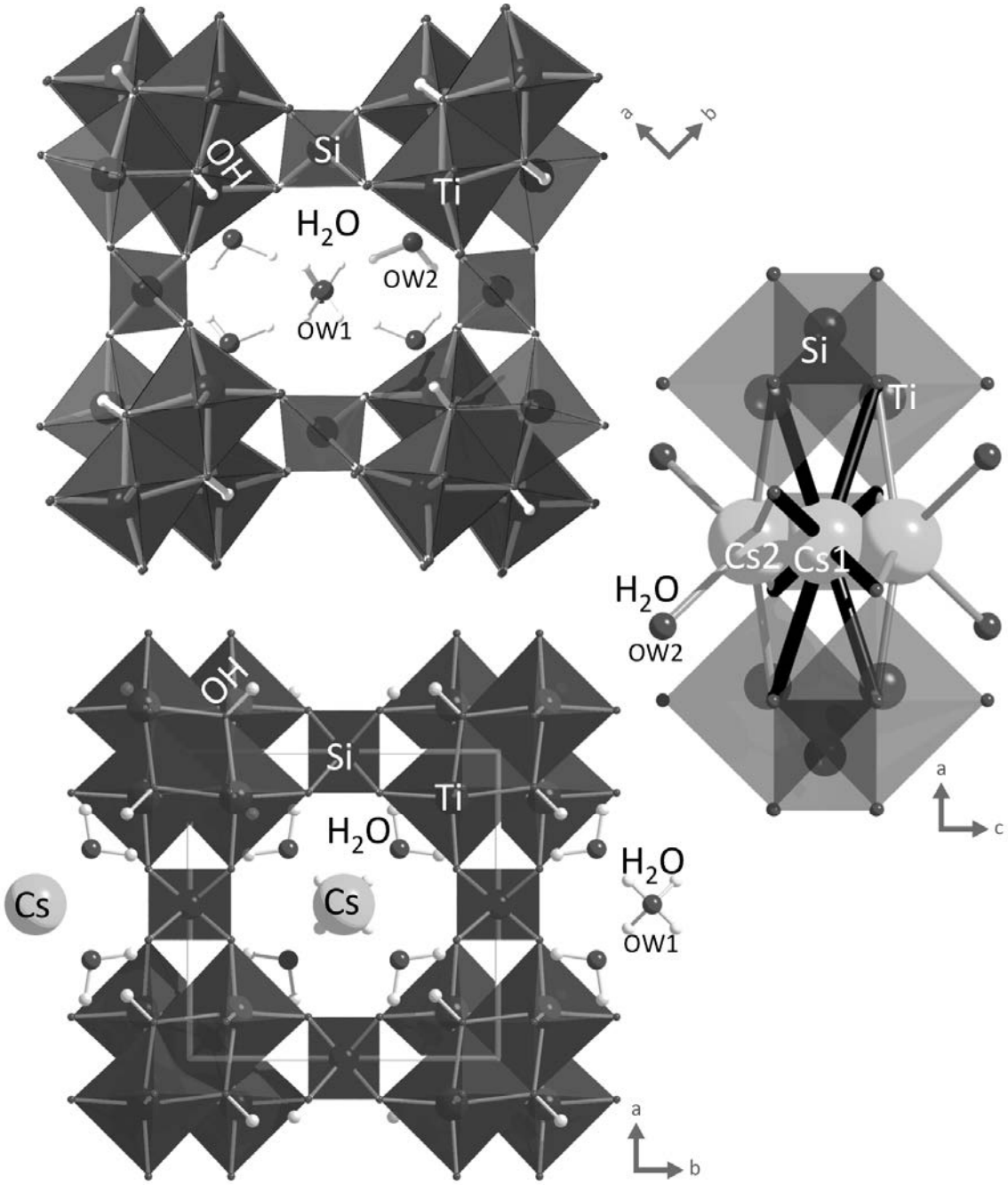

303

304 **FIGURE 1.** The crystal structure of sitinakite. (Top) view along [001] showing elliptical 8MR geometry, and H_2O
305 and OH positions in sitinakite-H. (Bottom) view along [001] showing circular 8MR geometry and Cs, H_2O, and OH
306 in sitinakite-HCs where Cs was removed on the right-hand side to reveal the orientation of disordered H_2O. (Right)
307 cross-section view of the 8MR showing the two crystallographic Cs sites.

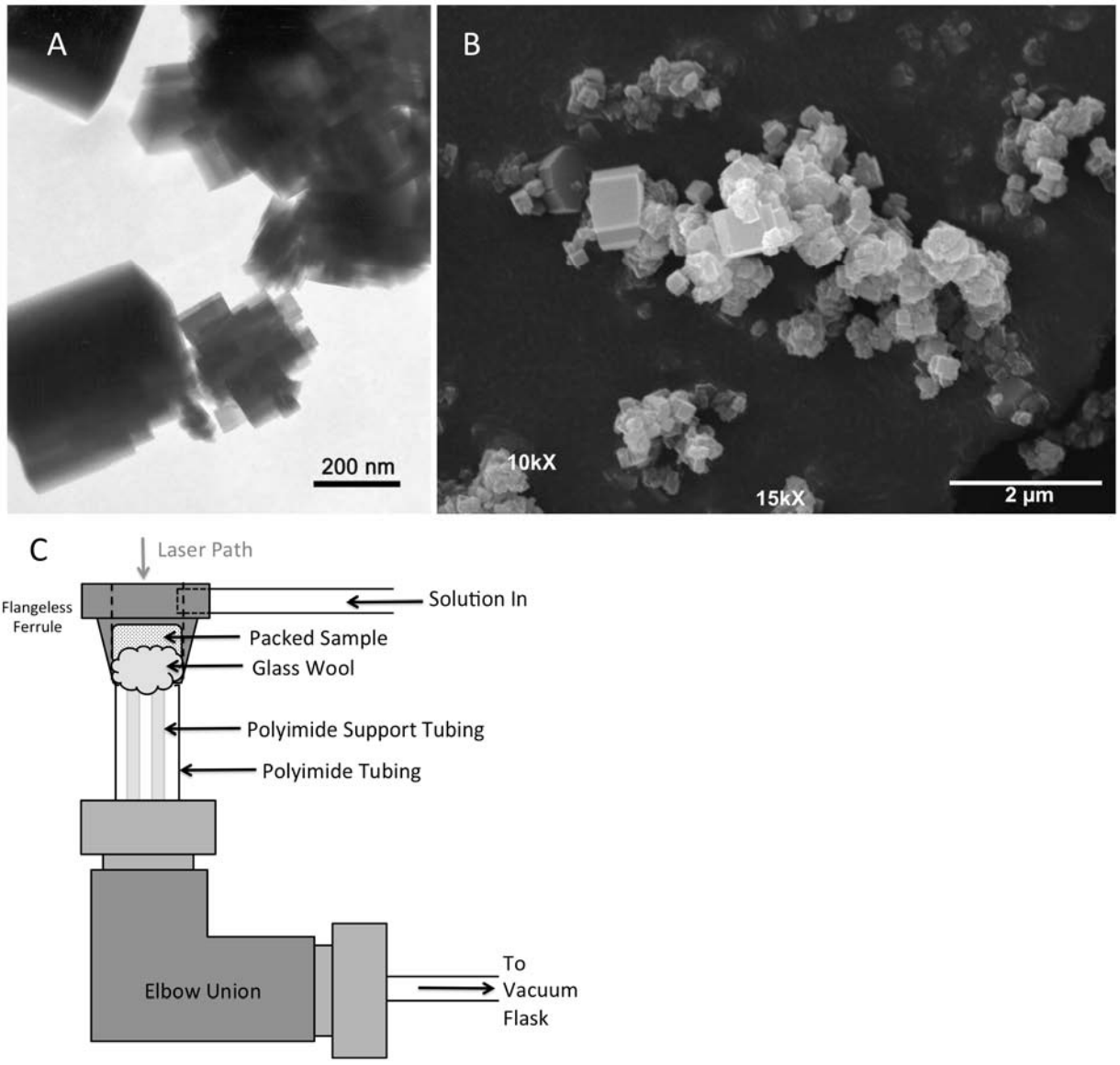

308

309 **FIGURE 2.** Transmission (A) and scanning (B) electron images of the as-synthesized material. (C) Schematic of the

310 environmental cell for in situ micro-Raman spectroscopy studies.

311

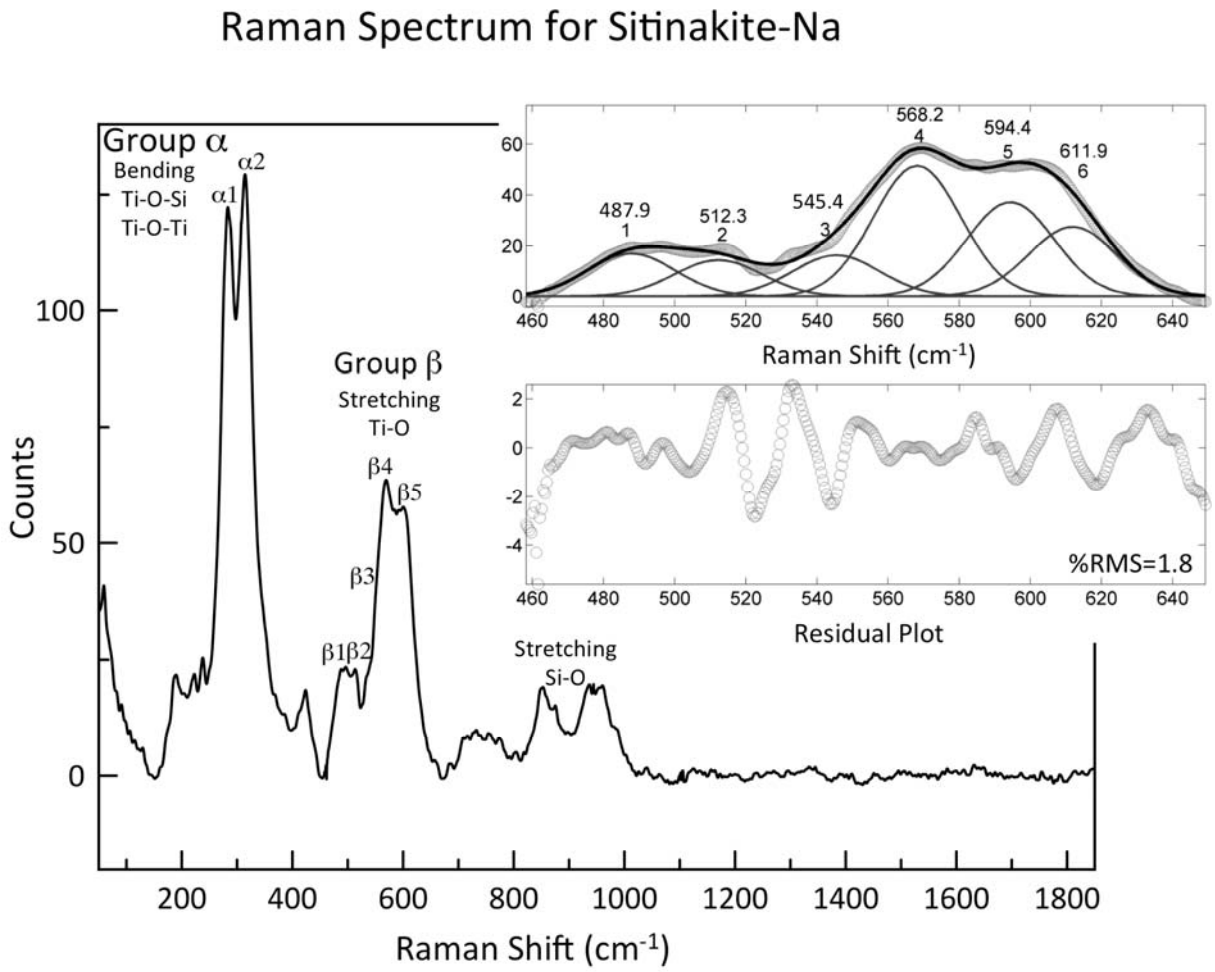

312

313 **FIGURE 3.** Example Raman spectrum for sitinakite-Na with the primary Groups α and β labeled. Inset shows the
314 results of the peak fitting for Groupβ, where each peak is labeled with its fitted peak position (in wavenumbers) and
315 peak number. Unlabeled peaks above 650 cm^{-1} are likely due to Si-O stretching.

316

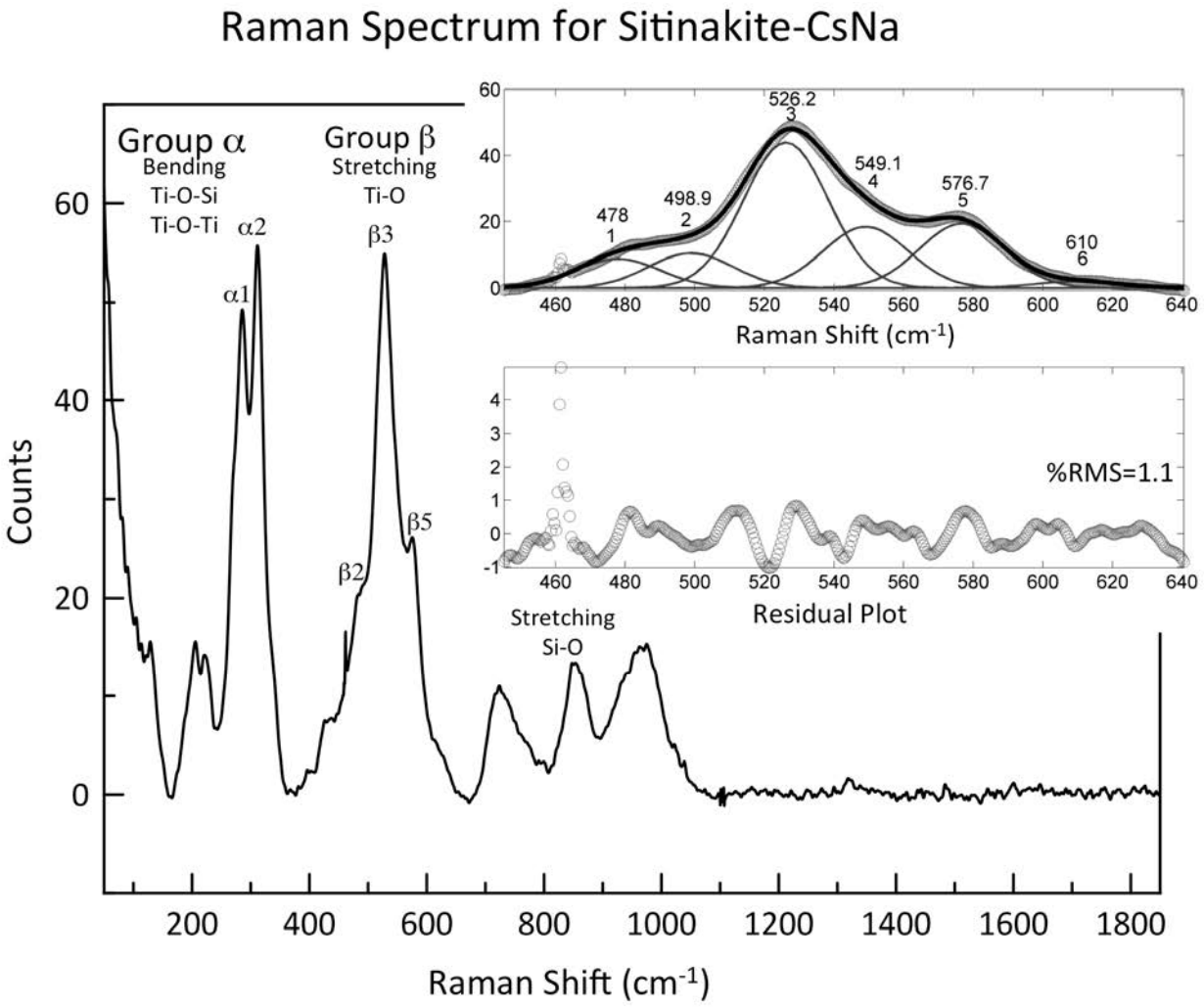

317

318 **FIGURE 4.** Example Raman spectrum for sitinakite-NaCs with the primary Groups α and β labeled. Inset shows the
319 results of the peak fitting for the Groupβ, where each peak is labeled with its fitted peak position (in wavenumbers)
320 and peak number. Unlabeled peaks above 650 cm^{-1} are likely due to Si-O stretching. Sharp peak at approximately
321 460 cm^{-1} is due to bad pixels on the CCD.

322

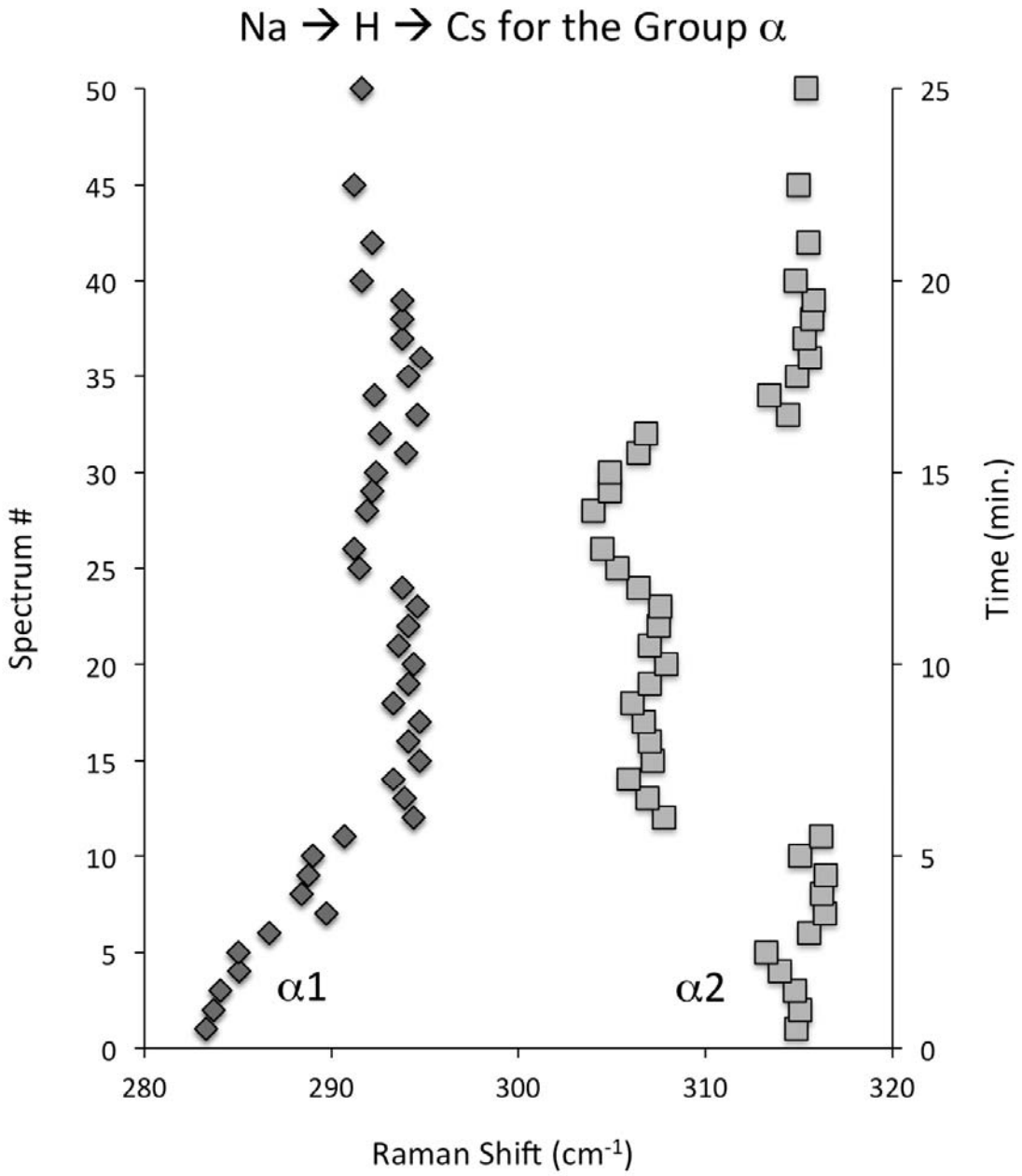

323

324 **FIGURE 5.** Peaks α1 and α2 for the Na→H→Cs ion exchange experiment. For the first 10 spectra, peak α1
325 gradually increases to 294.4 cm^{-1} while α2 remains relatively constant. After spectrum 10, α1 stops increasing and
326 remains constant at approx. 294.4 cm^{-1}, while α2 rapidly decreases to 308.5 cm^{-1}. After spectrum 30, α1 gradually
327 decreases to approx. 291.8 cm^{-1} and α2 increases to 316.7 cm^{-1}. Error bars are smaller than data symbols.

328

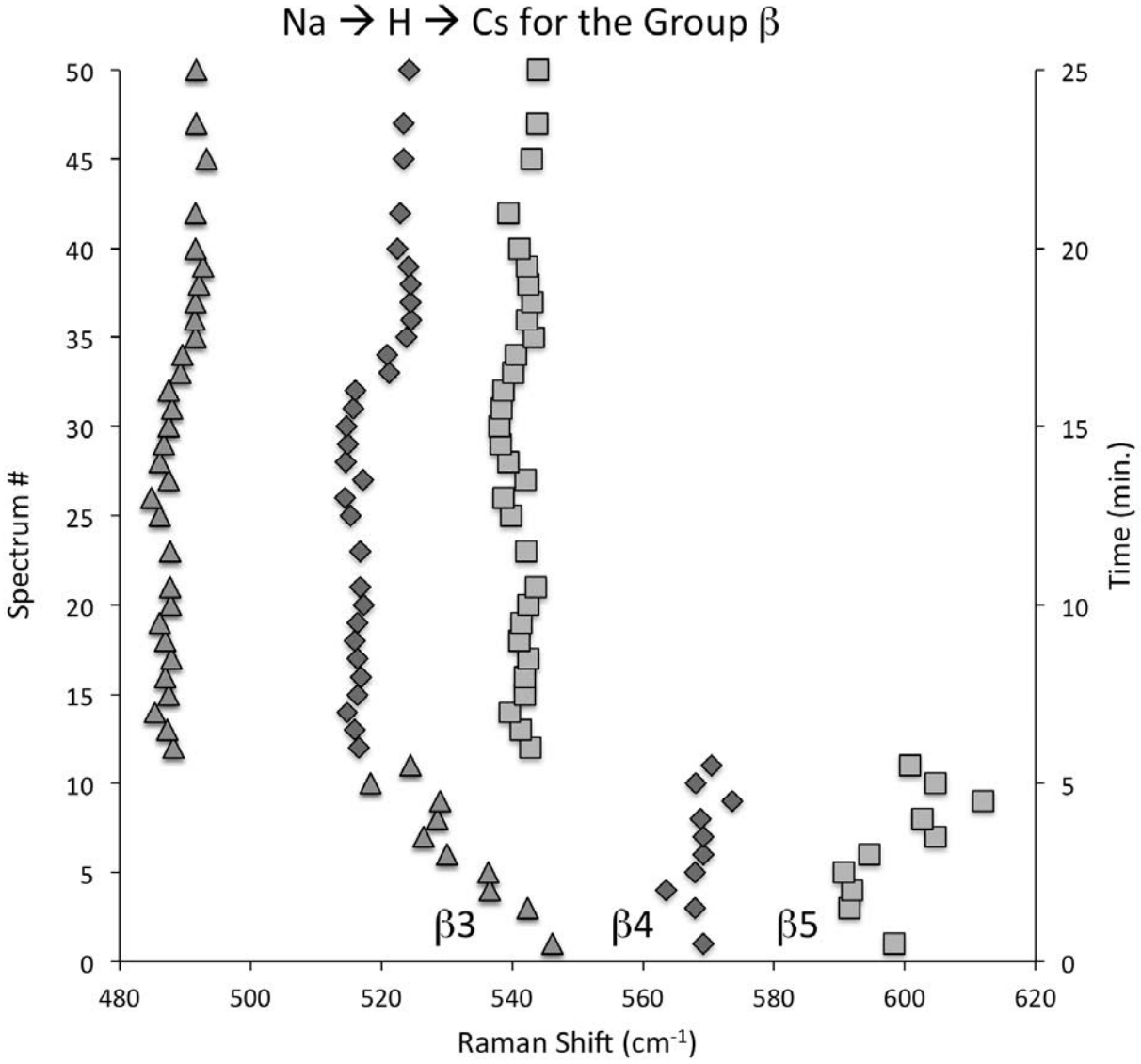

329

330 **FIGURE 6**. Peaks positions of the most intense peaks in Group β (β3, β4, and β5) for the Na→H→Cs ion exchange.
331 Peak β3 shows a continuous shift to lower wavenumbers during the first 10 spectra as deionized H_2O is passed
332 through the sample, while peak β5 shows a continuous increase in wavenumbers. After 10, HCl reached the sample
333 and sitinakite rapidly ion exchanged as shown by the red shift of all the peaks. Error bars are smaller than data
334 symbols.

335

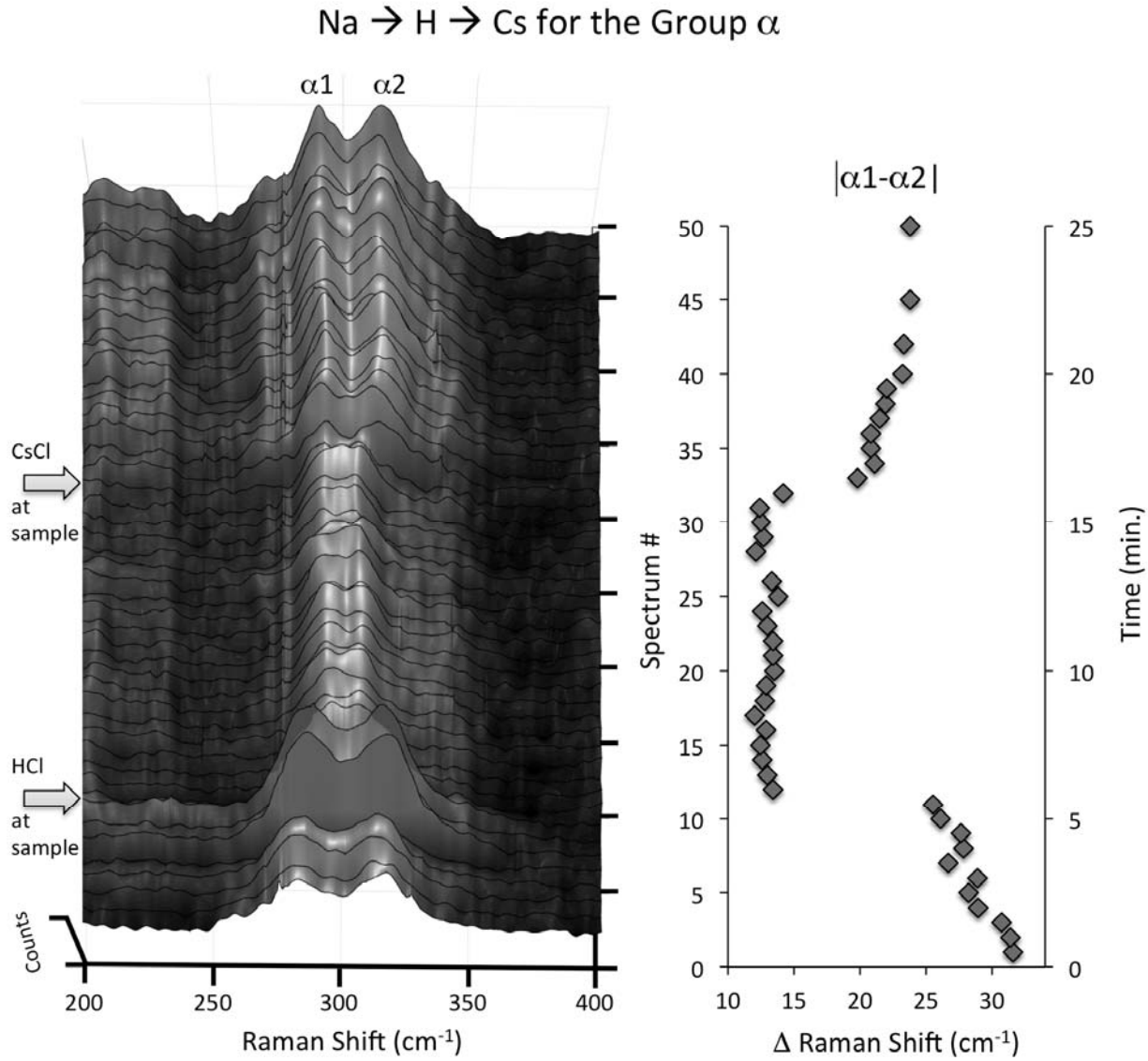

FIGURE 7. Stacked Raman spectra of Group α for the Na→H→Cs ion exchange. Graph on the right shows the |α1-α2| peaks as a function of time. Error bars are smaller than data symbols. Movement of relative peak positions indicates changes occurring in the 8MR geometry prior to H exchange for the first 10 spectra. After spectrum 10 the peaks moved closer to each other and remained fixed until the CsCl solution reached the sample at spectrum 32. After spectrum 33 |α1-α2| moved further apart and remained as such until spectrum 36, when the |α1-α2| began to increase again until spectrum 50, and then they held constant for an additional 350 spectra.

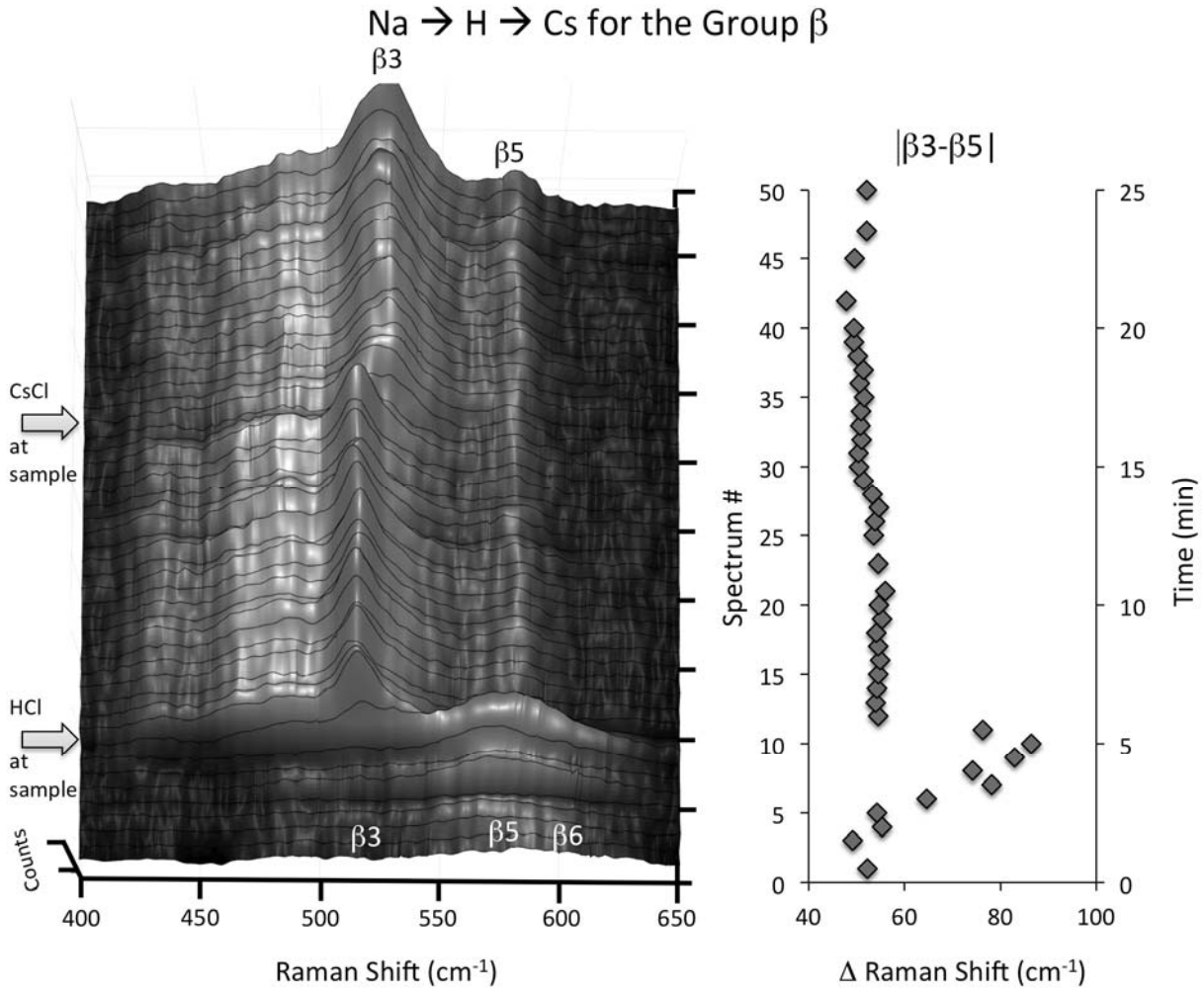

FIGURE 8. Stacked Raman spectra of Group β for the Na→H→Cs ion exchange. Graph on the right shows the |β□-β5| peaks as a function of time. Error bars are smaller than data symbols. See explanation in Figure 8 and in the text.

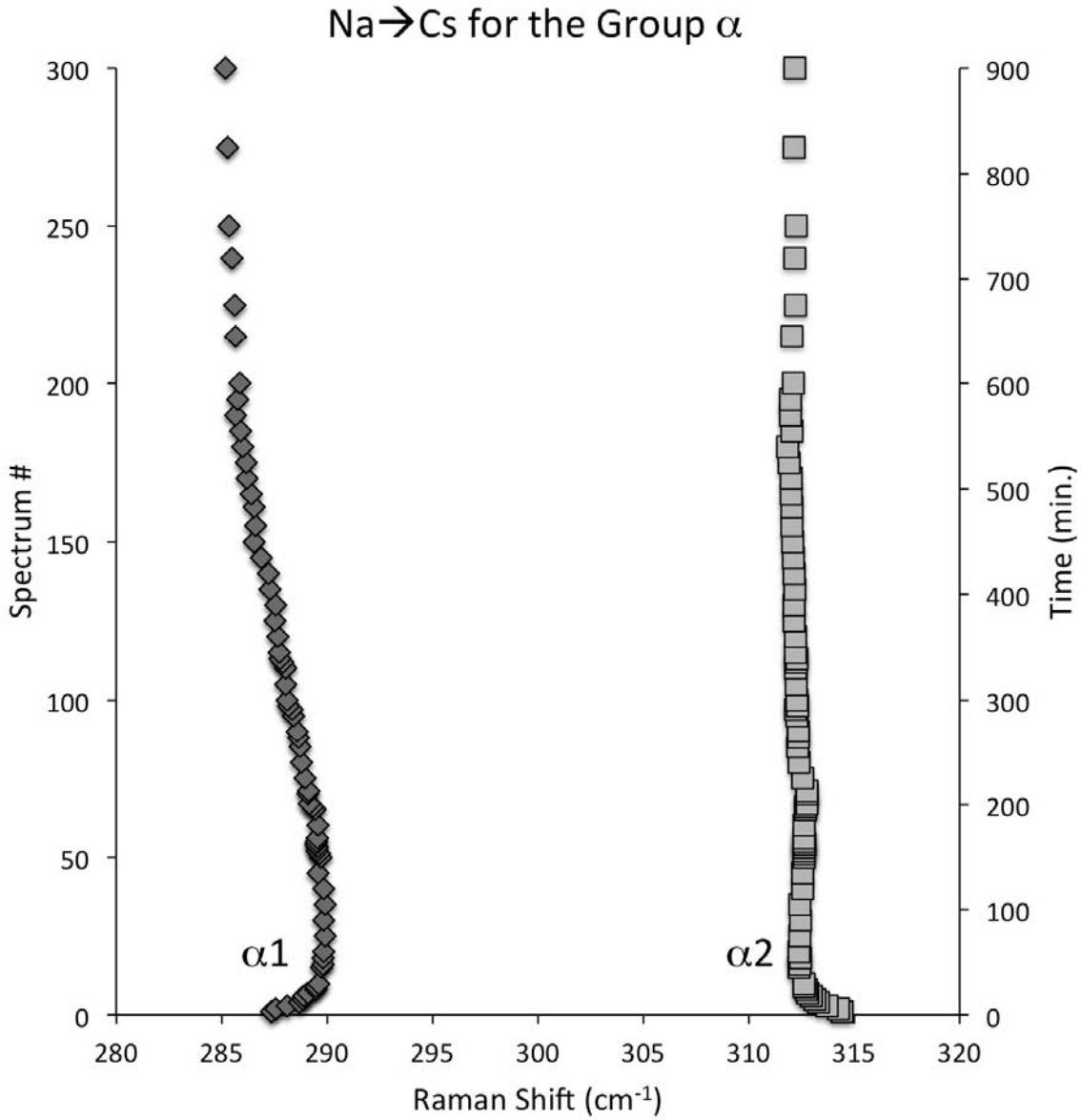

FIGURE 9. Peaks α1 and α2 through time for the Na→Cs ion exchange experiment. Error bars are smaller than data symbols.

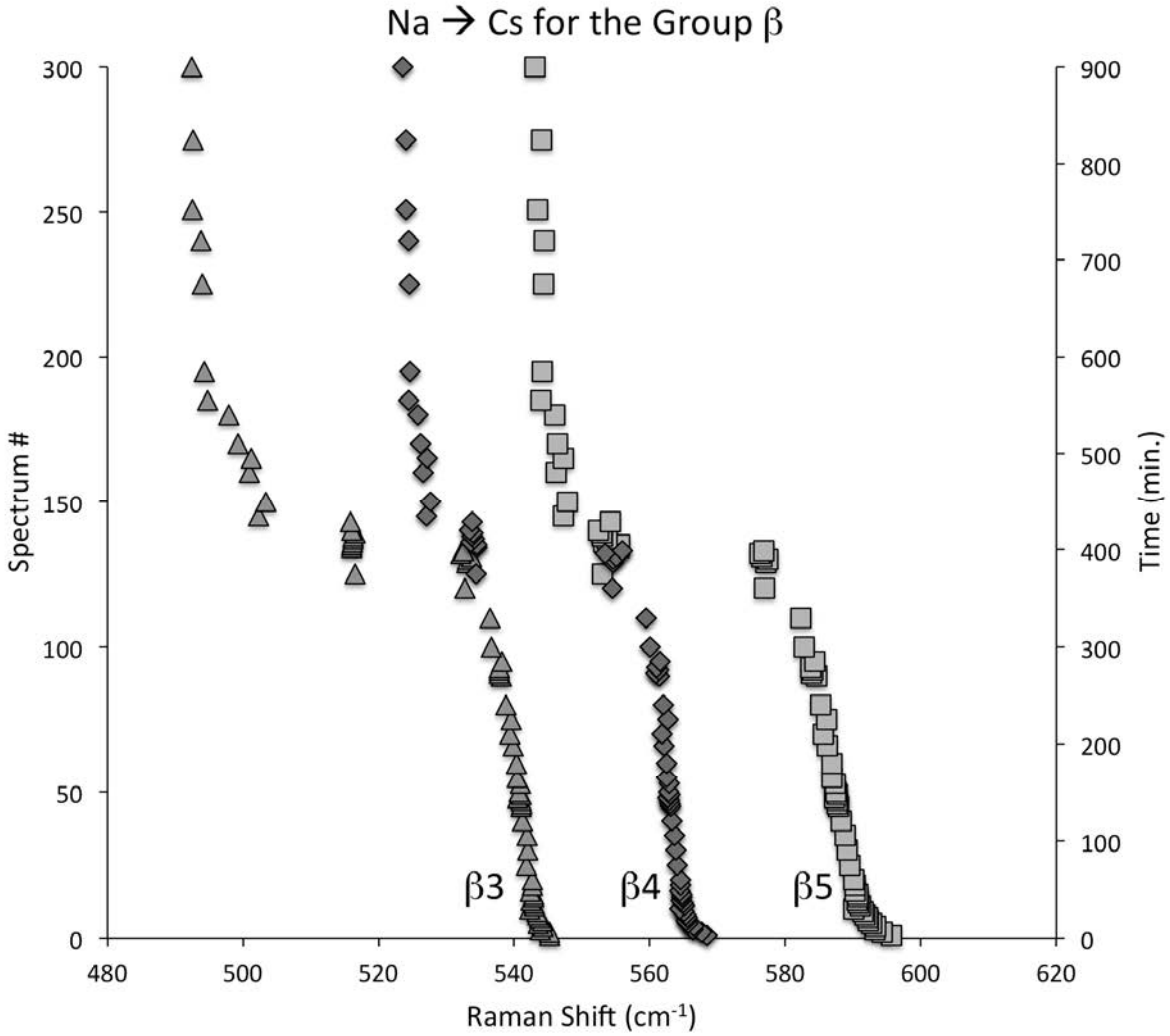

353

354

355 **FIGURE 10**. Peaks positions of the most intense peaks in Group β (β3, β4, and β5) through time for the Na→Cs ion

356 exchange. Error bars are smaller than data symbols.

357

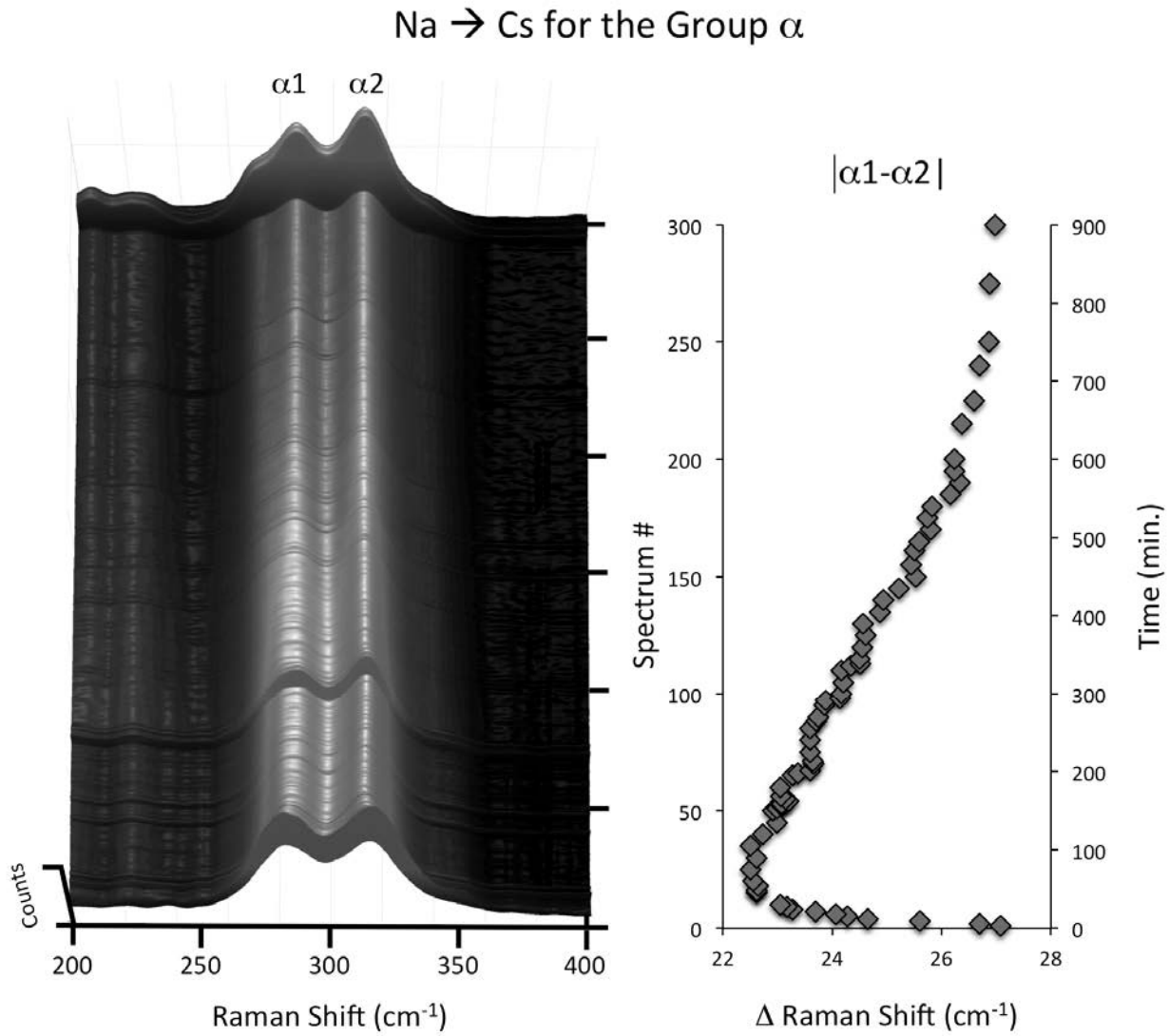

FIGURE 11. Stacked Raman spectra of Group α for the Na→Cs ion exchange. Graph on the right shows the |α1-α2| peaks as a function of time. Error bars are smaller than data symbols. For □α1-α2|, there were two major changes in the curve. First, there was a shift to lower wavenumbers from the start of the experiment to spectrum 40. Second, a gradual shift to higher wavenumbers occurred after from 40 to spectrum 400 (end of the experiment).

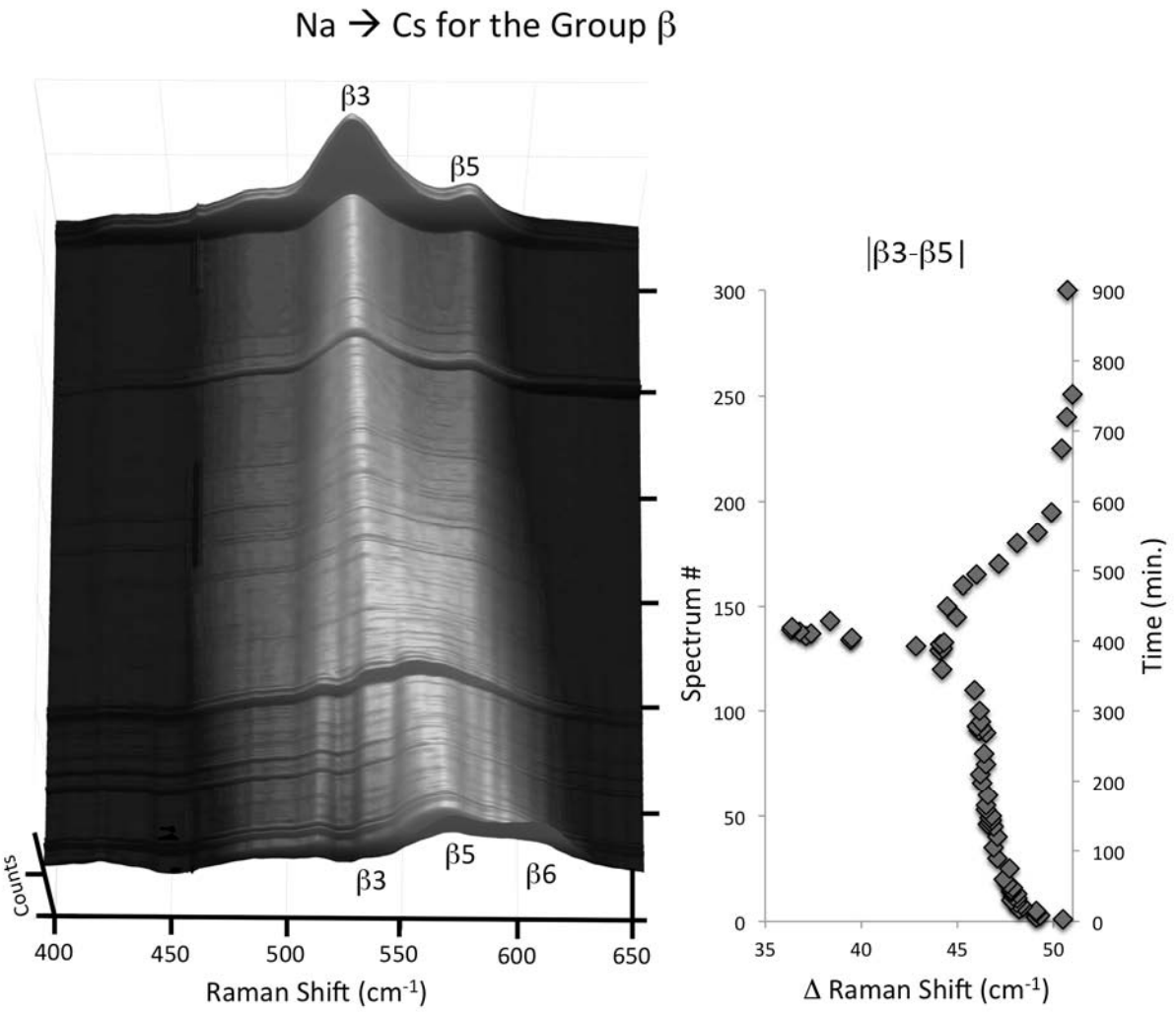

364

365 **FIGURE 12.** Stacked Raman spectra of Group β for the Na→Cs ion exchange. Graph on the right shows the |β3-β5|
366 peaks as a function of time. Error bars are smaller than data symbols. There are four major changes in the |β3-β5|
367 curve. First there was a graduate shift to lower wavenumbers from the onset of the experiment to spectrum 110.
368 Second, a rapid shift to lower wavenumbers occurred from spectrum 110 to spectrum 140. Third, there was again a
369 rapid shift to higher wavenumbers from spectrum 140 to spectrum 150. The final change was marked by a change
370 in the |β3-β5| curve slope after spectrum 150 until the end of the experiment. Spectra 300 to 400 are not shown as
371 there were no measurable changes in the |β3-β5| positions. Note that the initial and final |β3-β5| are nearly identical
372 and that there were up to four transient polyhedral distortions occurring in the sitinakite framework during Cs ion
373 exchange.

374

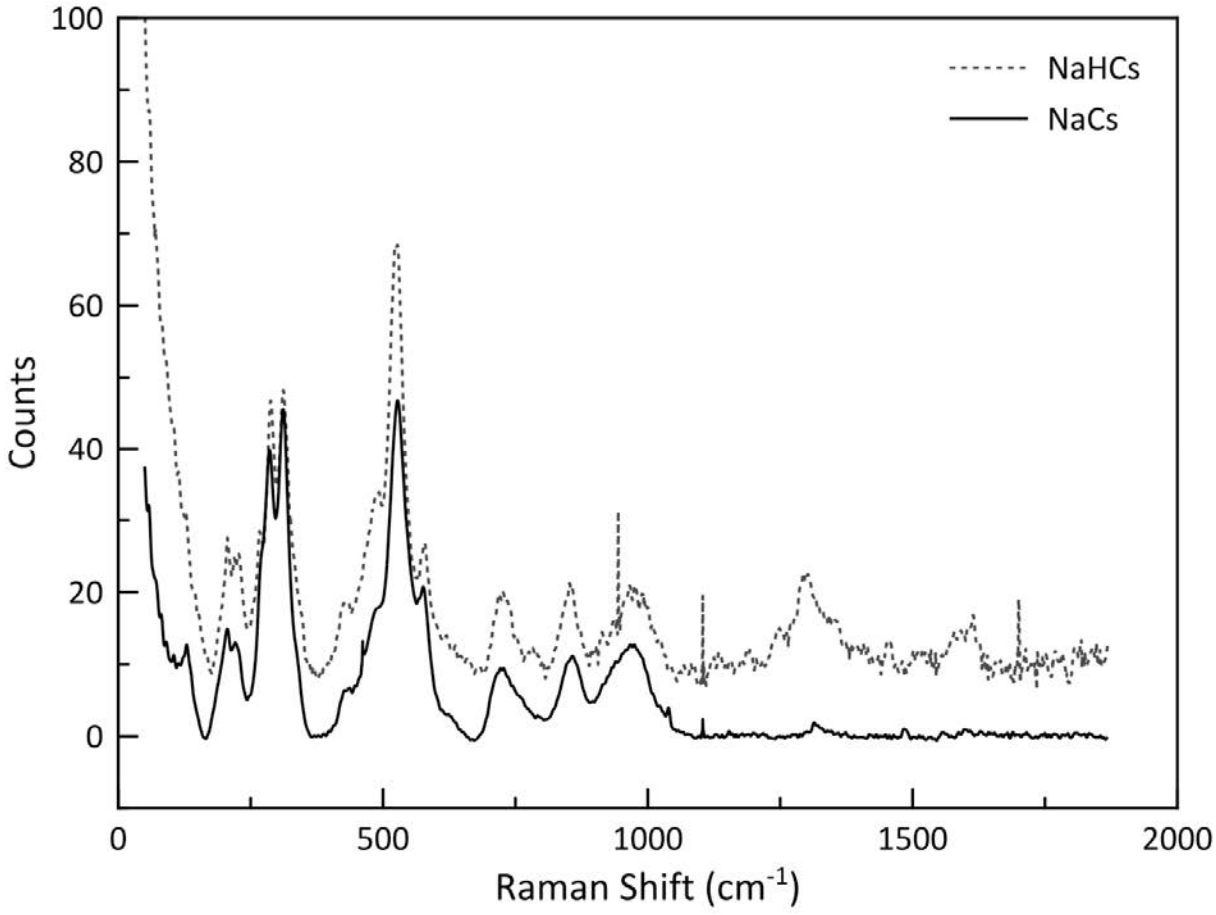

375

376 **FIGURE 13.** Raman spectra plot (with NaHCs having a 10 count offset along the y-axis) of the final exchanged
377 sitinakite forms for the difference ion exchange paths (Na→H→Cs dashed profile, Na→Cs solid profile) showing
378 the similarity between the two spectra. Sharp peaks at approximately 460 cm^{-1}, 930 cm^{-1}, and 1095 cm^{-1} are artifacts
379 of bad pixels on the CCD.

380

381

Table of TiO_6 Octahedral Geometry For the Sitinakite Forms

Compositional Form	Sitinakite-Na	Sitinakite-CsNa	Sitinakite-NaH	Sitinakite-NaHCs
Space Group	$P4_2/mcm$	$P4_2/mcm$	$P4_2/mbc$	$P4_2/mcm$
Distortion Index*	0.02499	0.02881	0.08608	0.0795
Quadratic Elongation*	1.0077	1.0078	1.0497	1.0416
Bond Angle Variance ($°^2$)*	23.012	23.19	139.111	117.893
Ave. Bond Length (Å)	2.008	2.008	1.979	1.986

382 * see VESTA (Momma and Izumi, 2011) user manual (http://jp-minerals.org/vesta/en/doc.html, last accessed

383 December 11, 2012).

384 **TABLE 1.**

385

386

Andrew, C.R., Yeom, H., Valentine, J.S., Karlsson, B.G., Bonander, N., Vanpouderoyen, G., Canters, G.W., Loehr, T.M., and Sandersloehr, J. (1994) Raman-spectroscopy as an indicator of Cu-S bond-length in type-1 and type-2 copper cysteinate proteins. Journal of the American Chemical Society, 116(25), 11489-11498.

Anthony, R.G., Dosch, R.G., Gu, D., and Philip, C.V. (1994) Use of Silicotitanates for Removing Cesium and Strontium from Defense Waste. Industrial & Engineering Chemistry Research, 33(11), 2702-2705.

Anthony, R.G., Dosch, R.G., and Philip, C.V. (1995) Method of using novel silico-titanates. Sandia Corporation, United States of America, patent 6110378.

Anthony, R.G., Dosch, R.G., and Philip, C.V. (2002) Silico-titanates and their methods of making and using. The Texas A&M University System, Sandia Corporation, United States of America, patent 6479427.

Arroyabe, E., Prechtel, F., Tobbens, D.M., Kaindl, R., and Kahlenberg, V. (2011) $K_2Ca_3Si_3O_{10}$, a novel trisilicate: high-pressure synthesis, structural, spectroscopic and computational studies. European Journal of Mineralogy, 23(3), 425-435.

Celestian, A.J., and Clearfield, A. (2007) The origin of ion exchange selectivity in a porous framework titanium silicate. Journal of Materials Chemistry, 17(46), 4839-4842.

Celestian, A.J., Kubicki, J.D., Hanson, J., Clearfield, A., and Parise, J.B. (2008) The mechanism responsible for extraordinary Cs ion selectivity in crystalline silicotitanate. Journal of the American Chemical Society, 130(35), 11689-11694.

Celestian, A.J., Medvedev, D.G., Tripathi, A., Parise, J.B., and Clearfield, A. (2005) Optimizing synthesis of $Na_2Ti_2SiO_7 \cdot 2H_2O$ (Na-CST) and ion exchange pathways for $Cs_{0.4}H_{1.6}Ti_2SiO_7 \cdot H_2O$ (Cs-CST) determined from in situ synchrotron X-ray powder diffraction. Nuclear Instruments & Methods in Physics Research Section B-Beam Interactions with Materials and Atoms, 238(1-4), 61-69.

Celestian, A.J., Parise, J.B., and Clearfield, A. (2010) In-situ structural studies of crystal growth in titanium silicates. Springer Handbook of Crystal Growth, 1637-1632.

Celestian, A.J., Parise, J.B., Smith, R.I., Toby, B.H., and Clearfield, A. (2007) Role of the hydroxyl-water hydrogen-bond network in structural transitions and selectivity toward cesium in $Cs_{0.38}(D_{1.08}H_{0.54})SiTi_2O_7 \cdot (D_{0.86}H_{0.14})_2O$ crystalline silicotitanate. Inorganic Chemistry, 46(4), 1081-1089.

Cherry, B.R., Nyman, M., and Alam, T.M. (2004) Investigation of cation environment and framework changes in silicotitanate exchange materials using solid-state Na-23, Si-29 and Cs-133 MAS NMR. Journal of Solid State Chemistry, 177(6), 2079-2093.

Chitra, S., Viswanathan, S., Rao, S.V.S., and Sinha, P.K. (2011) Uptake of cesium and strontium by crystalline silicotitanates from radioactive wastes. Journal of Radioanalytical and Nuclear Chemistry, 287(3), 955-960.

Ferdov, S., Lin, Z., Ferreira, R.A.S., and Correia, M.R. (2008) Hydrothermal synthesis, structural, and spectroscopic studies of vanadium substituted ETS-4. Microporous and Mesoporous Materials, 110(2-3), 436-441.

Galloway, M.M., Celestian, A.J., Parise, J.B., Clearfield, A., and Perry, H.P. (2006) Temperature stability of a molecular sieve crystalline silicotitanate with the mineral sitinakite topology. Abstracts of Papers of the American Chemical Society, 231.

Hess, N.J., Su, Y.L., and Balmer, M.L. (2001) Evidence of edge-sharing TiO_5 polyhedra in Ti-substituted pollucite, $CsTi_xAl_{1-x}Si_2O_{6+x/2}$. Journal of Physical Chemistry B, 105(29), 6805-6811.

Huang, E., Chen, C.H., Huang, T., Lin, E.H., and Xu, J.A. (2000) Raman spectroscopic characteristics of Mg-Fe-Ca pyroxenes. American Mineralogist, 85(3-4), 473-479.

Kaindl, R., Tobbens, D.M., and Kahlenberg, V. (2011) DFT-aided interpretation of the Raman spectra of the polymorphic forms of $Y_2Si_2O_7$. Journal of Raman Spectroscopy, 42(1), 78-85.

Kaindl, R., Tobbens, D.M., Penner, S., Bielz, T., Soisuwan, S., and Klotzer, B. (2012) Quantum mechanical calculations of the vibrational spectra of quartz- and rutile-type GeO_2. Physics and Chemistry of Minerals, 39(1), 47-55.

Kostov-Kytin, V., Mihailova, B., Kalvachev, Y., and Tarassov, M. (2005) Atomic arrangements in amorphous sodium titanosilicate precursor powders. Microporous and Mesoporous Materials, 86(1-3), 223-230.

Liu, H.W., Yang, D.J., Waclawik, E.R., Ke, X.B., Zheng, Z.F., Zhu, H.Y., and Frost, R.L. (2010) A Raman spectroscopic study on the active site of sodium cations in the structure of $Na_2Ti_3O_7$ during the adsorption of Sr^{2+} and Ba^{2+} cations. Journal of Raman Spectroscopy, 41(12), 1792-1796.

Luca, V., Hanna, J.V., Smith, M.E., James, M., Mitchell, D.R.G., and Bartlett, J.R. (2002) Nb-substitution and Cs^+ ion-exchange in the titanosilicate sitinakite. Microporous and Mesoporous Materials, 55(1), 1-13.

Medvedev, D.G., Tripathi, A., Clearfield, A., Celestian, A.J., Parise, J.B., and Hanson, J. (2004) Crystallization of sodium titanium silicate with sitinakite topology: Evolution from the sodium nonatitanate phase. Chemistry of Materials, 16(19), 3659-3666.

Menshikov, Y.P., Sokolova, E.V., Yegorov-Tismenko, Y.K., Khomyakov, A.P., and Polezhaeva, L.I. (1992) Sitinakite $Na_2KTi_4Si_2O_{13}(OH) \cdot 4H_2O$ - a new mineral. Zapiski Vsesoyuznogo Mineralogicheskogo Obshchestvo, 121(1), 94-99.

Mihailova, B., Valtchev, V., Mintova, S., and Konstantinov, L. (1996) Vibrational spectra of ETS-4 and ETS-10. Zeolites, 16(1), 22-24.

Milne, N.A., Griffith, C.S., Hanna, J.V., Skyllas-Kazacos, M., and Luca, V. (2006) Lithium intercalation into the titanosilicate sitinakite. Chemistry of Materials, 18(14), 3192-3202.

Momma, K., and Izumi, F. (2011) VESTA 3 for three-dimensional visualization of crystal, volumetric and morphology data. Journal of Applied Crystallography, 44, 1272-1276.

Nash, M.J., Rykov, S., Lobo, R.F., Doren, D.J., and Wachs, I. (2007) Photocatalytic activity of vanadium-substituted ETS-10. Journal of Physical Chemistry C, 111(19), 7029-7037.

Pavel, C.C., Zibrowius, B., Loffler, E., and Schmidt, W. (2007) On the influence of ion exchange on the local structure of the titanosilicate ETS-10. Physical Chemistry Chemical Physics, 9(26), 3440-3446.

Pertierra, P., Salvado, M.A., Garcia-Granda, S., Bortun, A.I., and Clearfield, A. (1999) Neutron powder diffraction study of $Ti\text{-}2(OH)_2OSiO_4 \cdot 1.5H_2O$. Inorganic Chemistry, 38(11), 2563-2566.

Poojary, D.M., Bortun, A.I., Bortun, L.N., and Clearfield, A. (1996) Structural studies on the ion-exchanged phases of a porous titanosilicate, $Na_2Ti_2O_3SiO_4 \cdot 2H_2O$. Inorganic Chemistry, 35(21), 6131-6139.

Poojary, D.M., Cahill, R.A., and Clearfield, A. (1994) Synthesis, Crystal-Structures, and Ion-Exchange Properties of a Novel Porous Titanosilicate. Chemistry of Materials, 6(12), 2364-2368.

Ricchiardi, G., Damin, A., Bordiga, S., Lamberti, C., Spano, G., Rivetti, F., and Zecchina, A. (2001) Vibrational structure of titanium silicate catalysts. A spectroscopic and theoretical study. Journal of the American Chemical Society, 123(46), 11409-11419.

Savitzky, A., and Golay, M.J.E. (1964) Smoothing and Differentiation of Data by Simplified Least Squares Procedures. Analytical Chemistry, 36(8), 1627-1639.

Smit, C., van Swaaij, R.A.C.M.M., Donker, H., Petit, A.M.H.N., Kessels, W.M.M., and Van de Sanden, M.C.M. (2003). Determining the material structure of microcrystalline silicon from Raman spectra. Journal of Applied Physics, 94(5), 3582-3588.

Southon, P.D., and Howe, R.F. (2002) Spectroscopic studies of disorder in the microporous titanosilicate ETS-10. Chemistry of Materials, 14(10), 4209-4218.

Su, Y., Balmer, M.L., and Bunker, B.C. (2000) Raman spectroscopic studies of silicotitanates. Journal of Physical Chemistry B, 104(34), 8160-8169.

Thorogood, G.J., Kennedy, B.J., Griffith, C.S., Elcombe, M.M., Avdeev, M., Hanna, J.V., Thorogood, S.K., and Luca, V. (2010) Structure and Phase Transformations in the Titanosilicate, Sitinakite. The Importance of Water. Chemistry of Materials, 22(14), 4222-4231.

Tobbens, D.M., and Kahlenberg, V. (2011) Improved DFT calculation of Raman spectra of silicates. Vibrational Spectroscopy, 56(2), 265-272.

Tripathi, A., Medvedev, D.G., and Clearfield, A. (2005) The crystal structures of strontium exchanged sodium titanosilicates in relation to selectivity for nuclear waste treatment. Journal of Solid State Chemistry, 178(1), 253-261.

Wang, H.W., and Bish, D.L. (2012) Infrared spectroscopic characterization of dehydration and accompanying phase transition behaviors in NAT-topology zeolites. Physics and Chemistry of Minerals, 39(4), 277-293.

Wilmarth, W.R., Lumetta, G.J., Johnson, M.E., Poirier, M.R., Thompson, M.C., Suggs, P.C., and Machara, N.P. (2011) Review: Waste-Pretreatment Technologies for Remediation of Legacy Defense Nuclear Wastes. Solvent Extraction and Ion Exchange, 29(1), 1-48.

Zhang, Z., Goodall, J.B.M., Brown, S., Karlsson, L., Clark, R.J.H., Hutchison, J.L., Rehman, I.U., and Darr, J.A. (2010) Continuous hydrothermal synthesis of extensive 2D sodium titanate ($Na_2Ti_3O_7$) nano-sheets. Dalton Transactions, 39(3), 711-714.

Zheng, Z.X., Gu, D., Anthony, R.G., and Klavetter, E. (1995) Estimation of Cesium Ion-Exchange Distribution Coefficients for Concentrated Electrolytic Solutions When Using Crystalline Silicotitanates. Industrial & Engineering Chemistry Research, 34(6), 2142-2147.